PERGAMON

Journal of Structural Geology 23 (2001) 1203–1214

JOURNAL OF STRUCTURAL GEOLOGY

www.elsevier.nl/locate/jstrugeo

The nucleation and evolution of Riedel shear zones as deformation bands in porous sandstone

S.G. Ahlgren

GeoStructure Group, Department of Geosciences, University of Arizona, Tucson, AZ 85721, USA

Received 17 May 1999; accepted 21 November 2000

Abstract

The term *Riedel shear zone* refers to a geometric fracture pattern commonly associated with strike–slip fault systems. Using field mapping and three-dimensional digital modeling, the progressive temporal evolution of natural Riedel shear zones within exposures of the Jurassic Navajo Sandstone is interpreted from the spatial evolution of small-scale, incipient Proto-Riedel Zones (PRZs) to more completely developed systems. PRZs nucleate as a tabular zone of localized shearing marked by en échelon deformation bands, each of which is no more than a few mm wide and tens of cm long. These initial deformation bands have an opposite (antithetic) sense of slip with respect to the zone, and are oriented at an acute angle of 55–85° to the trend of the zone. With increasing strain, deformation bands and sedimentary markers become sheared through granular flow across the zone and assume a sigmoidal form. Subsequent bands develop as conjugate shear fractures within the strain-hardened axis of the PRZ. These *antithetic driven* systems are not directly linked to pre-existing or external structural elements and are not compatible with traditional *synthetic driven* models of Riedel shear zones.

Keywords: Navajo sandstone; Riedel shear zone; Deformation band; Waterpocket fold; Utah

1. Introduction

This paper documents the spatial and temporal evolution of Riedel shear zones in porous sandstone from field examples in southern Utah. Although some of the fundamental concepts explored in this paper are not new, the synthesis of these ideas in the context of a naturally deformed structural system and the application of advanced visualization techniques may shed light on this particularly complex and interesting fault pattern.

1.1. Background

The term 'Riedel Shears' (Hills, 1963) refers to a specific fault geometry first created in clay cake models (Riedel, 1929). The pattern includes relatively short, en échelon fault segments that may link to form a through-going Principal Shear Zone (PSZ) (Skempton, 1966). Numerous workers have subsequently generated the Riedel pattern through clay cake experiments (e.g. Cloos, 1955; Morgenstern and Tchalenko, 1967; Tchalenko, 1968; Hildebrand-Mittlefehldt, 1979; Gamond, 1983; Maltman, 1987), direct shear experiments (e.g. Mandl et al., 1977; Bartlett et al., 1981; Schreurs, 1994), triaxial experiments (e.g. Marone and Scholz, 1989; Morrow and Byerlee, 1989), and through computer simulations (Dresan, 1991; Braun, 1994; McKinnon and Garrido de la Barra, 1998). Many workers document Riedel shear zones in natural systems ranging from regional scale (e.g. Tchalenko and Ambraseys, 1970; Moore, 1979; Moore and Byerlee, 1992) to outcrop scale (e.g. Dengo and Logan, 1979; Davis, 1996; Garcia and Davis, 1997) to thin section scale (e.g. Morgenstern and Tchalenko, 1967; Tchalenko, 1968; Maltman, 1987).

Riedel shear zones are found in dip–slip fault regimes (Dengo and Logan, 1979; Garcia and Davis, 1997) although the pattern is generally assumed to form in the cover sequence overlying some planar 'basement' wrench-fault system (as in the wrench-fault block models of Tanner, 1962; Wilcox et al., 1973; Moore, 1979). Smaller-scale Riedel shear zones are generally associated with a larger-scale Riedel shear zone system (e.g. Davis, 1996) or found within confined fault zones (as in the gouge experiments of Moore and Byerleee, 1991).

Geometrically, the idealized Riedel pattern is defined by a series of fractures oriented at specific angles to the trend of the PSZ (Fig. 1). The idealized system includes conjugate R and R' shear fractures, inclined at $45° \pm \phi/2$ (ϕ is the internal friction angle of the host rock), a P shear, inclined

E-mail address: ahlgren@geo.arizona.edu (S.G. Ahlgren).

0191-8141/01/$ - see front matter
PII: S0191-8141(00)00183-8

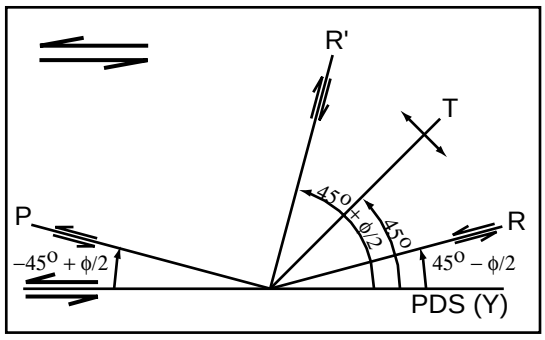

Fig. 1. Idealized Riedel shear zone geometry. ϕ is the angle of internal friction of the host rock. Principal Displacement Shears (PDSs) form sub-parallel to the trend of the zone.

at $-45° + \phi/2$, and a *T* fracture, inclined at 45° (e.g. Bartlett et al., 1981, fig. 3). Some workers report *X* shears, oriented at $-45° - \phi/2$ (Bartlett et al., 1981), but these shears are not considered in this study. The *R* and *P* shears exhibit a synthetic sense of shear with respect to the PSZ, R' shears exhibit an antithetic sense of shear (terminology after Wilcox et al., 1973) with respect to the PSZ, and *T* fractures are purely tensional features (e.g. Skempton, 1966; Bartlett et al., 1981). Some shear fractures may be sub-parallel to the trend of the PSZ and are alternatively termed 'Principal Displacement Shears' (PDS) (Skempton, 1966), *D* shears (Tchalenko, 1968) or *Y* shears (Bartlett et al., 1981). This study uses *R* to describe a synthetic shear, R' to describe an antithetic shear, and PDS to describe a shear oriented sub-parallel to the trend of the Riedel shear zone.

In natural systems, the angular relationships between individual shear surfaces and the PSZ is variable and dependent on a number of factors such as the strain rate and the stress state at the time of faulting. Localized elevated fluid pressure within a faulting region may result in reorientation of far-field principal stresses (e.g. Byerlee, 1990, 1992) causing synthetic and antithetic shears to be inclined more steeply with respect to the trend of the PSZ (e.g. Gamond, 1983; Naylor et al., 1986). Propagation of shears within the Riedel shear zone may also induce local stress field rotations, further influencing the types and geometry of developing shear fractures (e.g. Naylor et al., 1986; Mandl, 1988).

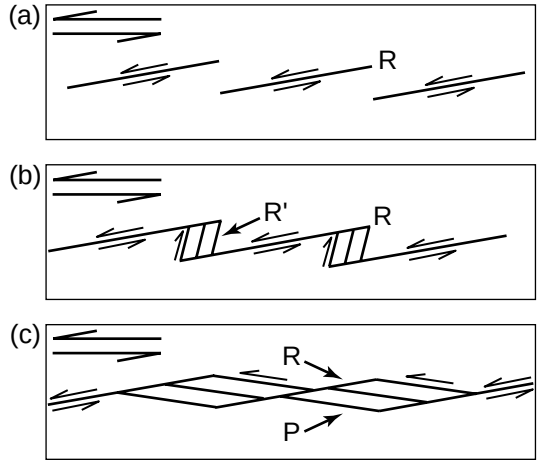

Fig. 2. The sequential development of a sinistral *synthetic driven* Riedel shear zone. (a) Zone initiates as en échelon *R* shears and in most systems, (b) antithetic R' shears develop, although in some systems, (c) *P* shears may develop.

The sequential development of shear surfaces within a natural Riedel system is poorly understood. In physical models and computer simulations, however, the sequential progression of shearing within Riedel shear zones is well constrained but dependent on modeling conditions. Generally speaking, the most widely accepted model for Riedel shear zone development is *synthetic driven* in the sense that lower-angle *R* and *P* shears generally pre-date higher-angle R' shears (Fig. 2). Most workers agree that *R* shears are the first or one of the first shears to form (e.g. Morgenstern and Tchalenko, 1967; Tchalenko, 1970; Bartlett et al., 1981), although *P* shears may also form first, especially in dilational systems (Moore and Byerlee, 1992). *R* and *P* shears may develop synchronously (Bartlett et al., 1981) or *P* shears may also develop later as links between *R* shears (Tchalenko, 1968; Moore and Byerlee, 1992). R' shears may develop concurrently with or postdate *R* shears (e.g. Tchalenko, 1968; Moore, 1979) and they are typically confined to the overlap zones between over-stepping *R* segments (e.g. Tchalenko, 1968). Most workers agree that PDSs are the last to develop (e.g. Tchalenko, 1968; Bartlett et al., 1981), although some computer modeling predicts that these shears actually form first (Braun, 1994). It is important to note that individual shears generally remain active after other types develop, thus strain within a Riedel shear zone is accommodated by synchronous movement on all fractures comprising the zone (e.g. McKinnon and Garrido de la Barra, 1998).

2. Location of study area and study methodology

This study examines outcropping Riedel shear zones in the Jurassic Navajo Sandstone of southern Utah. The primary study area is located near Sheets Gulch, a 2 km^2 region located along the eastern edge of Capitol Reef National Park (Fig. 3). Structural data from Sheets Gulch are compiled from previous field maps (Davis et al., 2000), 1:2400 and 1:600 mapping on aerial photographic base maps, and finer-scale outcrop mapping. Supporting data were also collected within the Navajo Sandstone exposed along the eastern edges of the San Rafael Swell and the East Kaibab Monocline.

3. Structural geometry

3.1. Regional-scale structure

Sheets Gulch is located between two Laramide uplifts,

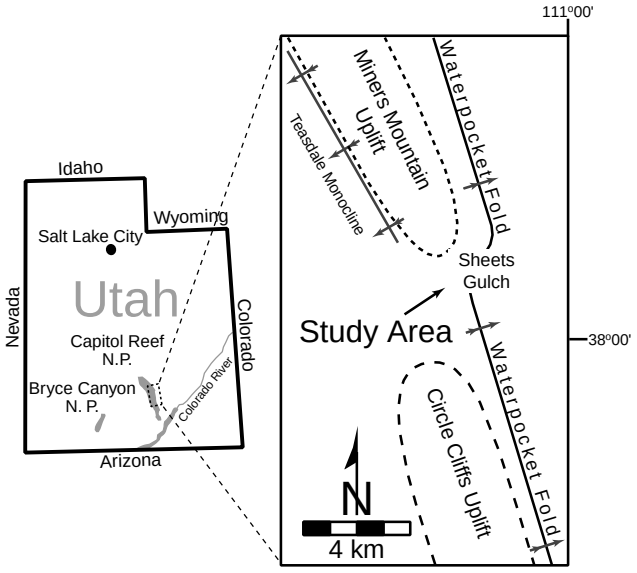

Fig. 3. Map of Utah showing location of Sheets Gulch and simplified structural geology of the study area. Modified after Billingsley et al. (1987).

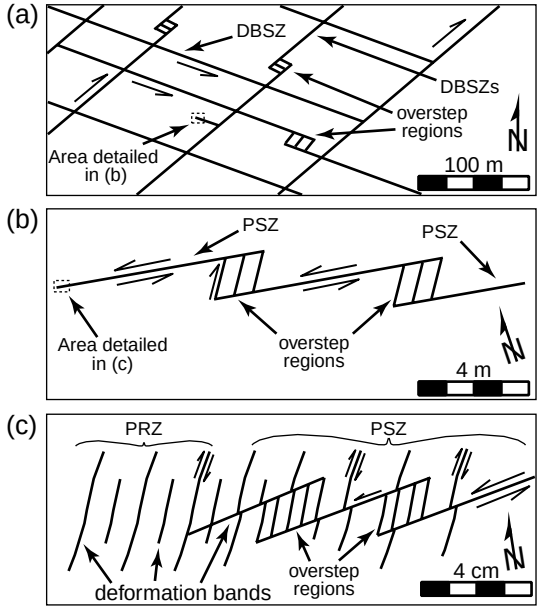

Fig. 4. Geometry and scale invariance of Riedel shear zones composed of deformation bands and systems of deformation bands. (a) Regional-scale deformation band shear zones (DBSZs) with overstep regions between adjacent DBSZs. (b) Outcrop-scale Principal Shear Zones (PSZs) with overstep regions between other smaller-scale PSZs. (c) Tip region of PSZ composed of individual deformation bands. The PSZ tips as a Proto-Riedel Zone (PRZ). Note: the relative orientation of the figure changes from (a) to (c).

the Circle Cliffs uplift to the south and the Miners Mountain uplift to the northwest (Kelley, 1955) (Fig. 3). The combined eastern flanks of these two uplifts is commonly referred to as the Waterpocket Fold, which changes from a steeply dipping, east-vergent monocline to the south of Sheets Gulch to a shallowly east-dipping homocline to the north of Sheets Gulch. Structurally, this region may represent a transfer zone between basement structure(s) controlling each of the uplifts, although the exact geometry of these basement structures is poorly known. Striking geometrical differences between the two uplifts, as expressed by the geometry of the Waterpocket Fold, suggest that the Circle Cliffs uplift is cored by an east-vergent reverse fault and the Miners Mountain uplift is cored by a southwest-vergent reverse fault (Bump et al., 1997). A complex transfer zone between the basement structures results in penetrative deformation within the cover rocks at Sheets Gulch.

The exposed supracrustal sequence comprises the eolian Jurassic Navajo Sandstone underlain by the shales and sandstones of the lower members of the Jurassic Glen Canyon Group, and overlain by shales and sandstones of the Jurassic San Rafael Group (Hintze, 1988). Of the exposed units, the Navajo Sandstone is inferred to be the most mechanically competent and brittle. It is also important to note that the Navajo Sandstone has a remarkably clean, quartz-rich composition (Kiersch, 1950) with an initial porosity of ~20% (e.g. Antonellini and Aydin, 1994).

The Navajo Sandstone within Sheets Gulch is penetratively deformed by a system of conjugate strike–slip deformation band shear zones (DBSZs) that formed during the initial development of the Waterpocket Fold (Davis et al., 1997, 2000). Although DBSZs may extend the breadth of the study area, measurable offset on an individual DBSZ is no more than 4 m and total regional strain accommodated on DBSZs may not exceed 2%. Dextral and sinistral DBSZs are mutually offsetting and there is no clear temporal relationship between DBSZs in the two orientations, thus they may have formed contemporaneously (Davis et al., 2000). Additionally, there is no correlation between the orientations of DBSZs and the orientations of regional joint sets, suggesting that DBSZs did not form through reactivation of pre-existing joints.

As seen in other Riedel systems (e.g. Morgenstern and Tchalenko, 1967) the system at Sheets Gulch displays a remarkable scale invariance and self-similarity over at least three orders of magnitude (Davis, 1996; Ahlgren, 1999) (Fig. 4). For example, regional-scale DBSZs may be interpreted as large-scale Riedel shear zones, sub-bands within the DBSZs often exhibit a Riedel geometry, and these bands, in turn, may be Riedel shear zones.

3.2. Outcrop-scale structure

This study examines the sequential development of outcrop-scale Riedel shear zones composed of deformation bands (Davis, 1996) marked by grain-scale cataclasis and compaction of the Navajo Sandstone (Aydin, 1978). Riedel array deformation bands may form as subsidiary shears associated with a regional-scale DBSZ, as a PSZ contained within a regional scale DBSZ, or within otherwise undisturbed host rock (Fig. 4). A majority of observed PSZs terminate at one end in undisturbed rock and at the other

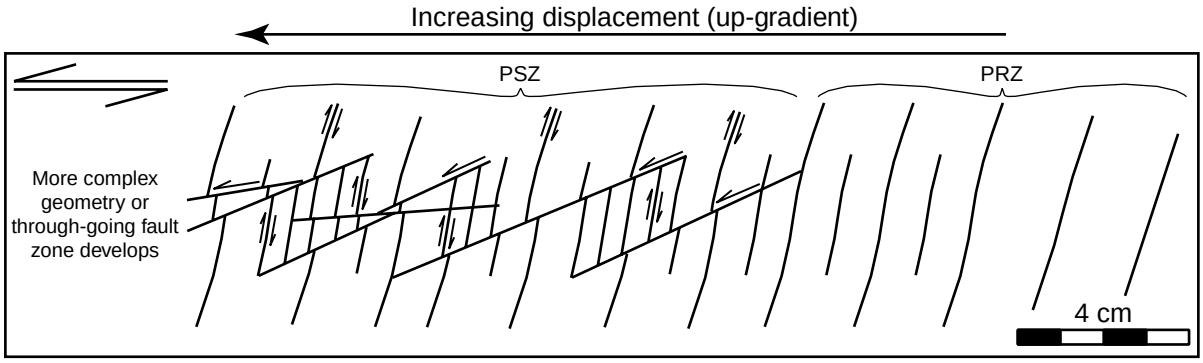

Fig. 5. Plan view of the tip region of an idealized sinistral PSZ showing systematic along-strike evolution from a PRZ to a PSZ to a more complex fault zone.

end at a PSZ or DBSZ, and tip-to-tip examples, with both ends of the zone terminating in otherwise undisturbed rock, are also present although uncommon.

The geometry and kinematics of Riedel shear zones are most easily interpreted from tip regions of evolving PSZs and from regions between adjacent, en échelon PSZs (Fig. 4). These regions tend to be geometrically simple and, kinematically, they provide a snapshot of zone development at a primitive stage. Deformation within the tip regions of a PSZ is interpreted as representing the lateral propagation mechanism of the PSZ as well as the original nucleation mechanism (thus the earliest stage of sequential development) of the PSZ. These regions of incipient Riedel array development are termed Proto-Riedel Zones (PRZs).

The following geometrical description of PRZs and PSZs uses nomenclature similar to Morgenstern and Tchalenko (1967) by which individual deformation band types are labeled $Z_1 \ldots Z_4$.

3.3. Geometry of Riedel shear zones

As observed within the Navajo Sandstone at Sheets Gulch and supported by observations at other localities, some

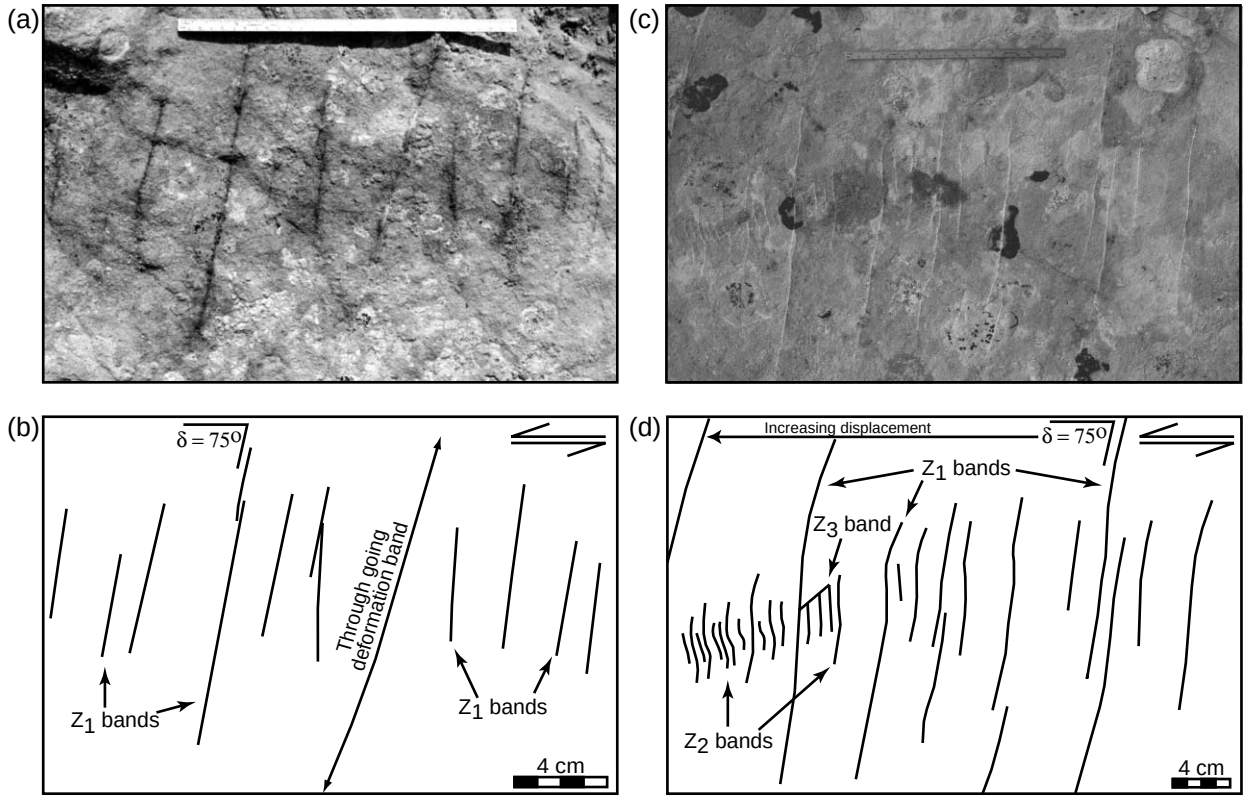

Fig. 6. Geometry of PRZs observed at Sheets Gulch. (a–b) Plan view of a sinistral PRZ composed entirely of en échelon Z_1 bands oriented at a high angle to the zone boundary ($\delta = 75°$). Note semi-regular spacing, linearity of Z_1 bands, and the lack of lower-angle bands. (c–d) Plan view of a sinistral PRZ composed primarily of Z_1 and Z_2 bands. Displacement grows toward the left side of the image and the PRZ evolves into a PSZ along strike. Note the regular Z_1 band spacing, in filling by Z_2 bands, sigmoidal form of Z_1 and Z_2 bands, and minor Z_3 band development.

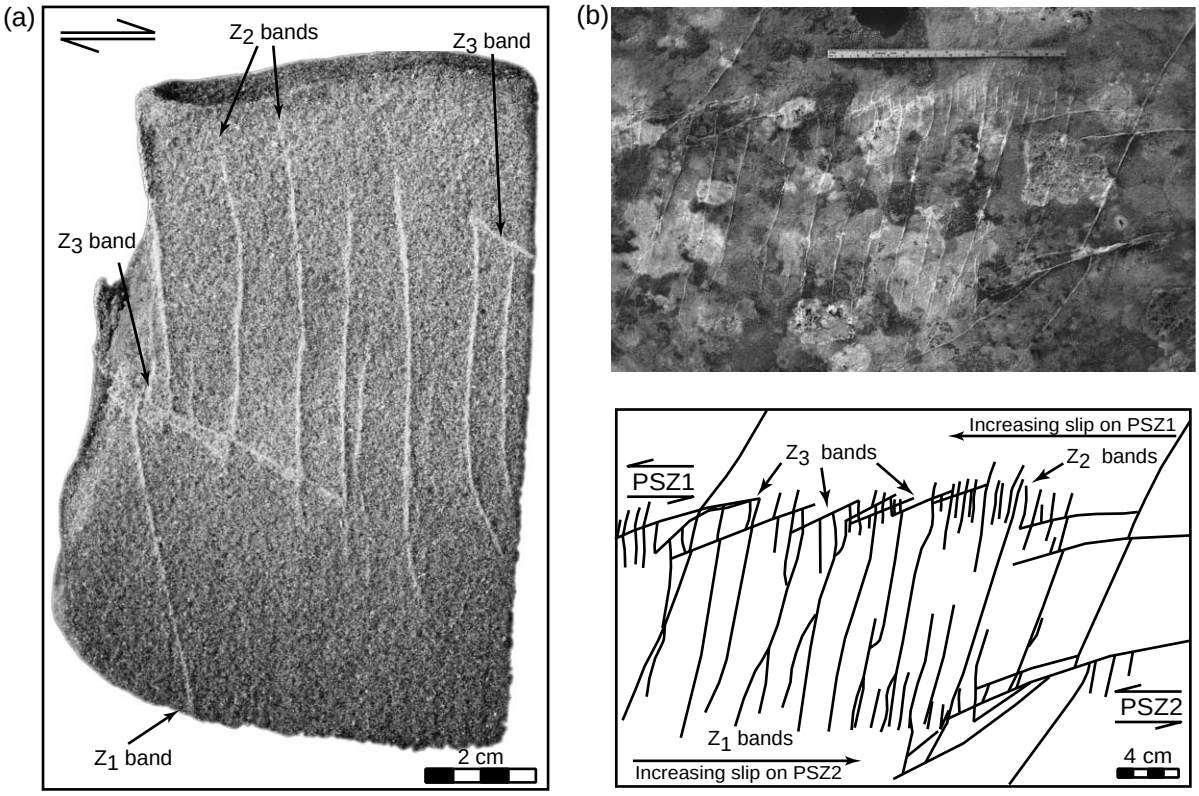

Fig. 7. Examples of observed overstep region geometries. (a) Photograph of a hand sample containing an open overstep region between two Z_3 bands. Note incomplete linking of sigmoidal Z_2 bands by lower-angle Z_3 bands. (b) Photograph and tracing of closed overstep region between PSZs tipping as PRZs. Note the regularly spaced Z_1 bands within the overstep zone and the lack of lower-angle bands within the overstep.

smaller-scale Riedel shear zones exhibit a systematic geometric change along strike from a PRZ to a well-developed PSZ (Fig. 5). Within Sheets Gulch, these zones are oriented similarly to regional scale DBSZs and are isolated (they do not connect with other structures), tip into DBSZs, or evolve into DBSZs along strike.

A PRZ is defined by a tabular zone of en échelon, planar to curviplanar, unconnected deformation bands (Z_1 bands) (Fig. 6). Spacing of the bands along strike of the PRZ is semi-regular, and on the order of a few cm. Z_1 bands are oriented at 50–88° (average 67° ± 11°, $n = 139$) with respect to the strike of the PRZ, are roughly symmetric about the PRZ axis, and extend laterally away from the axis of the zone for a few cm to tens of cm. Some PRZs are composed solely of spaced, en échelon Z_1 bands, which may be linear or sigmoidal in plan view (Fig. 6a–b).

Further away from the zone tip (e.g. Fig. 5), Z_1 bands typically have a gently curved, sigmoidal geometry in plan view, and a single Z_1 band may exhibit a 13–43° angular discordance between the strike of one its free tips and the strike of its interior region. Similarly, there may be a change in dip magnitude and/or direction from tip to tip along a single Z_1 band, suggesting that the band is slightly helicoidal in three dimensions. The Z_2 bands may be present in regions between adjacent Z_1 bands. If present, Z_2 bands are centered on the axis of the PRZ, typically sigmoidal in plan view, and oriented sub-parallel to Z_1 bands, at least near the axis of the PRZ (Fig. 6c–d).

Continuing along the PRZ away from the tip, lower-angle Z_3 deformation bands are typically present at 5–35° (average 19° ± 8°, $n = 92$) with respect to the strike of the PRZ. Z_3 bands typically offset both Z_1 and Z_2 bands with a sense of shear synthetic to displacement on the PRZ. In some examples, Z_3 bands link the tips of Z_2 bands, although there may be incomplete along-strike linking of the Z_1 and Z_2 bands comprising the PRZ (Fig. 7a). The tip-linking Z_3 bands may overstep and overlap in plan view, and within regions between adjacent, overlapping Z_3 segments, additional laterally discontinuous Z_4 deformation bands oriented at 40–114° (average 78° ± 15°, $n = 26$) with respect to the PRZ may be present. In plan view, Z_4 bands tend to be linear and oriented sub-parallel to Z_1 and Z_2 bands in the interior of the PRZ.

Moving still further along the zone, the system generally becomes too complicated for detailed geometric interpretation, although through-going deformation bands oriented sub-parallel to the trend of the PRZ are easily interpreted. Z_1, Z_2, Z_3, and Z_4 bands are often thicker with polished or slickenlined sides, suggesting that each band is now (spatially along strike of the PSZ) a brittle slip surface

(Aydin and Johnson, 1983). The sense of slip on Z_2 bands is synthetic to the sense of slip on the zone as a whole and the sense of slip on Z_1, Z_2, and Z_4 bands is antithetic with respect to the sense of slip on the zone as a whole. At this point (spatially), the PRZ may be considered a PSZ.

3.4. Geometry of overstep regions

Overstep regions are discrete, roughly orthorhombic regions where there is spatial overlap between pairs of deformation bands (commonly Z_3 bands) or band systems (PRZs or PSZs) (Davis, 1996). An overstep region is *closed* if the segments overlap and are connected by other bands or band systems (for example, Z_3 bands connected by Z_4 bands) and *open* otherwise (Fig. 7). All observed examples are *contractional* oversteps in which dextral bands or band systems step to the left, and sinistral bands or band systems step to the right (Segall and Pollard, 1980). In larger-scale systems, spacing between PSZs or DBSZs may be tens of cm to a few m, but in more primitive overstep systems between pairs of Z_3 bands or PRZs, spacing of the approaching segments is a few cm to 20 cm. Commonly, stepping Z_3 bands *do not* overlap spatially, and sigmoidal Z_2 bands are present within the overstepping region (Fig. 7a). It is important to note, however, that the Z_2 bands do not necessarily connect with the overstepping Z_3 bands, thus the Z_2 bands form part of the soft link between the Z_3 bands. In situations where Z_3 bands do overlap spatially, however, Z_4 bands are present and act as hard links between the Z_3 bands.

3.5. Summary of observed geometries

As described, some Riedel shear zones vary geometrically along strike from a PRZ, to a geometrically simple PSZ, to a more complex, through-going fault zone (e.g. Fig. 5). The tip region of a PRZ is typically composed of Z_1 deformation bands which tend to be regularly spaced and linear in plan view. Along strike toward the center of the zone, these Z_1 deformation bands may be sigmoidal in plan view and are overprinted by other elements including Z_2, Z_3, and Z_4 deformation bands. Still further along strike, the zone typically becomes geometrically complicated and detailed analysis is not possible.

4. Strain analysis

The consistent along-strike geometry of observed Riedel shear zones suggests that a PRZ accommodates a certain amount of shear strain prior to Z_3 band nucleation. For a given PRZ, it is possible to approximate the magnitude of shear strain it accommodates using a simple relationship between the shear strain, area change of the shear zone, and the change in orientation of a linear marker crossing the zone (Ramsay and Huber, 1987, eq. 26.4):

$$\cot \alpha' = \frac{\cot \alpha - \gamma}{1 + \Delta_A} \quad (1)$$

where α and α' are the angle of a linear feature with respect to the outside and inside walls of the shear zone, respectively, γ is the shear strain along the shear zone, and Δ_A is the area dilation of the shear zone. Simplifying for γ, the equation becomes

$$\gamma = \cot \alpha - (\cot \alpha')(1 + \Delta_A). \quad (2)$$

The amount of angular shear (ψ) is then calculated from γ using the simple relationship (Ramsay and Huber, 1983, p. 3)

$$\gamma = \tan(\psi). \quad (3)$$

In this study, the 'internal' strike of a Z_1 band (proximal to the PRZ axis) and its 'external' strike (distal from the PRZ axis) are used as α' and α values, respectively, and γ values are computed iteratively for a range of area changes.

Strain analysis of 13 PRZs from Sheets Gulch yields γ values ranging from 0 to 1.75 with an average γ of 0.31 ± 0.28 (Table 1). Corresponding ψ values range from 0 to 58° and average $22° \pm 14°$ ($n = 59$). Although there is great variability in shear strains calculated from different PRZs, γ and ψ values computed from multiple Z_1 bands contained within a single PRZ are reasonably consistent, and computed ψ values are compatible with observed angular rotations of deformation bands and sedimentary horizons across PRZs. These results suggest that a certain amount of angular shear may be accommodated along a PRZ preceding through-going deformation banding, although the magnitude of angular shear varies between PRZs.

5. Visualizing Riedel shear zones in three dimensions

To better understand the internal geometry of a Riedel shear zone, I reconstructed a field-sampled Riedel shear zone in three-dimensional digital space (Ahlgren, 1999). Previous workers have effectively applied methods such

Table 1
Results from strain analysis of 13 PRZs from Sheets Gulch. Note the small deviations of computed γ and ψ values computed for a single PRZ, but relative inconsistency between PRZs

PRZ	Offset sense	γ average	Std dev.	ψ average	Std dev.
AH-4	Sinistral	0.21	0.12	11.64	7.11
AH-7a	Sinistral	0.32	0.08	17.87	4.32
AH-8	Sinistral	0.19	0.11	10.93	6.15
AH-10	Sinistral	0.68	0.01	34.22	0.57
AH-11	Dextral	1.54	0.13	56.97	7.68
AH-12	Dextral	0.32	0.04	17.66	2.28
AH-15	Sinistral	0.78	0.01	37.87	0.37
AH-16	Sinistral	1.54	0.13	56.97	7.68
AH-19	Sinistral	0.31	0.11	17.46	6.02
AH-22	Sinistral	0.26	0.02	14.54	0.99
AH-23	Sinistral	0.50	0.01	26.63	0.74
AH-24	Sinistral	0.35	0.16	19.41	9.25
AH-42	Dextral	0.59	0.13	30.63	7.43

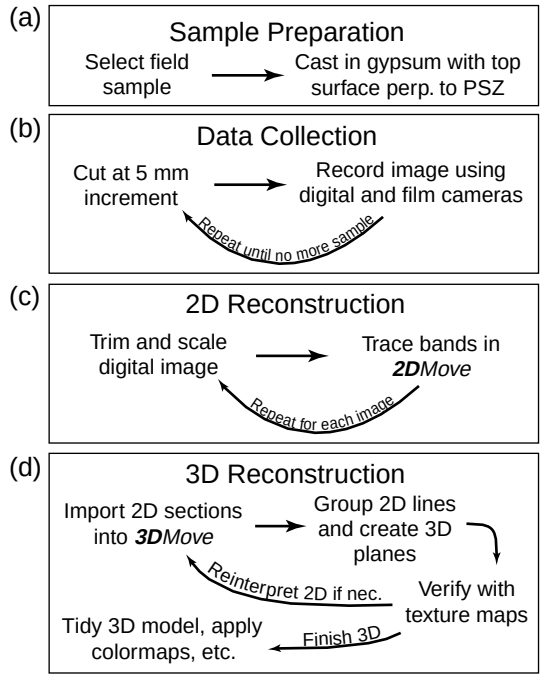

Fig. 8. Method for three-dimensional reconstruction of a PSZ. (a) First, the field sample is cast in a block of gypsum cement prior to (b) sequential dissection with a large rock saw. (c) Digital photographs from each slice of the sample are traced as cross sections in two dimensions. (d) The two-dimensional sections are then used to construct a three-dimensional digital model honoring the original structural geometry.

as computer-aided tomography to visualize the three-dimensional geometry of complex structures such as Riedel shear zones (e.g. Schreurs, 1994). Compared to other methods, sequential dissection is inexpensive and more accessible, but the original sample is completely destroyed.

The destructive modeling procedure includes sectioning, imaging, and digital reconstruction of a representative PSZ (Fig. 8). The sample was cast into a 35 cm × 25 cm × 25 cm block of gypsum cement and sliced sequentially at 5 mm intervals with a standard rock saw. Each freshly exposed rock surface was photographed with tripod-mounted digital and film cameras from an orthogonal distance of 65 cm. After digitally trimming and scaling the photographs, deformation band traces were digitized in a two-dimensional structural cross section balancing computer program, and these sequential cross sections and plan-view sections were imported into a three-dimensional structural restoration computer program.[1] Much like interpreting gridded seismic data, deformation band traces were correlated across adjacent vertical sections and verified by plan views (Fig. 9a). The final three-dimensional model includes approximately 40 vertical cross sections and three plan views, and unlike the original sample, the model facilitates full virtual tours through the heart of the PSZ (Fig. 9b). It is important to emphasize that the digital model is a *reconstruction* of the dissected field sample, not an *interpretation* of the dissected field sample.

The digital model supports and clarifies relationships gleaned from field observations. Because this particular field sample is not from the exact tip region of a PSZ (the sample is not a PRZ), all four types of deformation bands (Z_1, Z_2, Z_3, and Z_4) are present and each is geometrically similar to field examples. For example, Z_1 bands are sigmoidal in plan view and they are clearly helicoidal in three dimensions, with along-strike variability in dip magnitude and direction. In plan view, Z_2 bands are sigmoidal and sub-parallel to Z_1 bands, although they are not as laterally extensive as Z_1 bands. In cross section, Z_2 bands do not extend as deeply into the sample as Z_1 bands, and they exhibit a more subtle three-dimensional helicoidal geometry. Z_3 bands are relatively planar, oriented at smaller angles with respect to the PRZ, and clearly offset both Z_1 and Z_2 bands (note: these mm-scale offsets are not honored in the digital representation). Similarly, Z_4 bands are present in overlap zones between stepping Z_3 bands, but are not incorporated in the digital reconstruction due to their small size and geometric complexity.

6. Discussion of structure

The along-strike spatial continuum between a PRZ and a PSZ and the kinematic compatibility between components of the PRZ and the PSZ suggests that, with increasing strain, a PRZ evolves smoothly into a PSZ (Fig. 10). This variation in structural style is consistent with the along-strike displacement gradient observed in numerous field examples, with zero displacement at a zone tip and a maximum displacement near the center of the zone (for tip-to-tip examples) or at a junction with another zone. As suggested for similar systems (Pollard et al., 1982; Peacock, 1991) the changing along-strike morphology correlates with strain magnitude, thus the region with the lowest strain records the lowest-strain deformation mechanism(s). In some natural systems, these earliest features may not be clear due to overprinting by higher-strain features. Within the Navajo Sandstone, however, these initial features are captured as deformation bands within isolated PRZs, the tip regions of propagating PSZs, and the overstep regions between zones (Fig. 6).

The presence of PRZs comprising only Z_1 bands and the symmetry of deformational styles about the center of tip-to-tip PSZs suggests that Z_1 band formation is the earliest stage in the progressive development of PSZs. A PRZ nucleates as a tabular array of Z_1 bands and, if additional strain is necessary, the zone propagates laterally as a zone of Z_1 bands, while higher-strain elements evolve along strike toward the center of the zone. The formation of Riedel shear zones in this manner is incompatible with the traditional *synthetic driven* model of Riedel shear zone

[1] Two-dimensional cross sections and three-dimensional models created with *2DMove*™ and *3DMove*™, respectively, courtesy of Midland Valley Exploration, Glasgow, UK (see Gibbs, 1990; Gibbs and Griffiths, 1996).

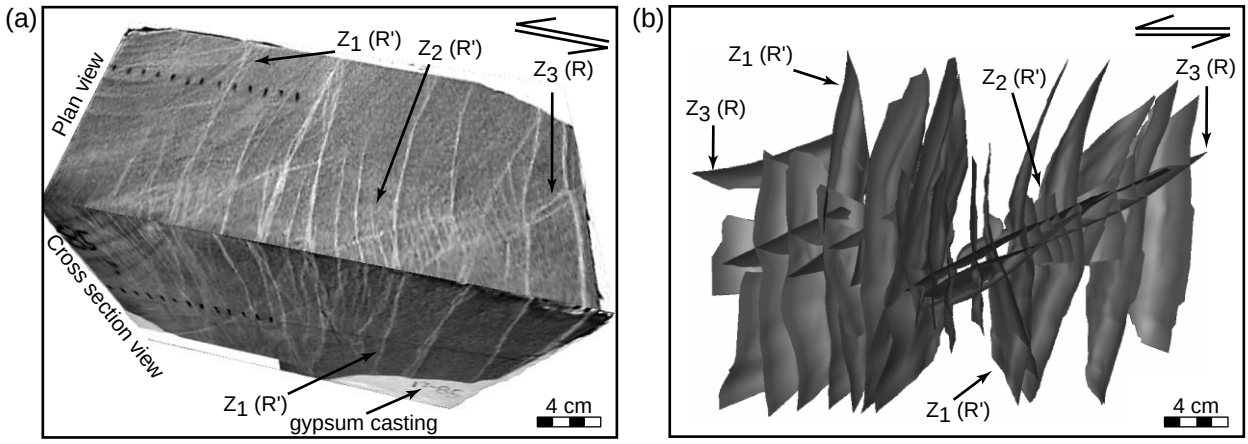

Fig. 9. Three-dimensional digital reconstruction of a sinistral PSZ. (a) Two-dimensional map and cross section views of the dissected field sample mapped into three dimensions. The light-colored lines are traces of deformation bands in the dissection planes. (b) Plan view of three-dimensional reconstruction of the PSZ. Surfaces are shaded according to relative depth within the model. Note: scale bars are approximate due to perspective view.

development documented in the literature. Rather, the preferred mode of array development observed in southern Utah is *antithetic driven*, in that Z_1 and Z_2 bands (which evolve into R' bands) initiate the brittle deformation process, are subsequently sheared, and are overprinted by a pair of conjugate Z_3 and Z_4 bands (which evolve into R and R' bands, respectively). With sufficient strain, the zone may evolve into a through-going fault zone (DBSZ).

6.1. Three-dimensional PSZ geometry

Both the three-dimensional digital PSZ reconstruction and field observations document the helicoidal geometry of shears comprising a Riedel array, which has been noted either directly or indirectly by other workers (e.g. Emmons, 1969; Wilcox et al., 1973; Moore, 1979; Naylor et al., 1986; Braun, 1994; Schreurs, 1994). It is important to note, however, that in these and other analog models, the synthetic shears exhibit a helicoidal morphology whereas the antithetic shears do not, as is documented in this study.

As suggested by analog modeling, a helicoidal fracture geometry may reflect a stress discontinuity from the base of the model to the free surface caused by shear stresses propagating upward from the 'basement,' with the fracture seeking some ideal orientation within the stress field (Naylor et al., 1986; Braun, 1994). Observed deformation within Sheets Gulch is confined to the structurally competent Navajo Sandstone and Davis et al. (2000) suggest

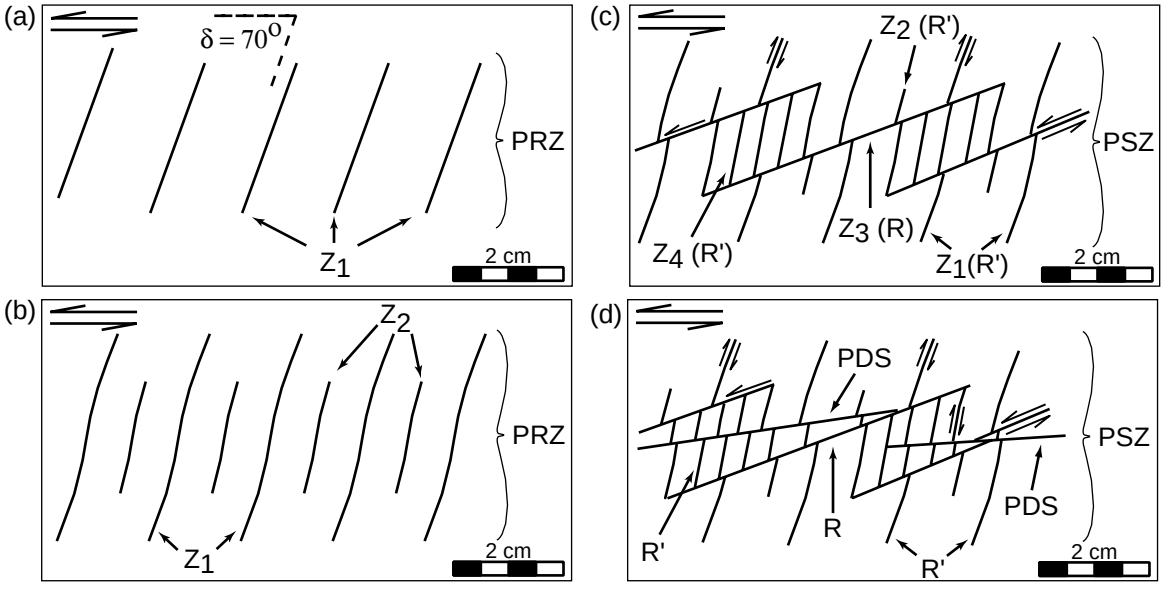

Fig. 10. The sequential development of an *antithetic driven* Riedel shear zone. (a) The zone initiates as PRZ composed of spaced Z_1 bands with $\delta = 70°$ (arbitrary). (b) Simple shear sigmoidally deforms Z_1 bands; Z_2 bands develop. (c) Z_3 (R) and Z_4 (R') bands form while shear occurs on Z_1 and Z_2 bands (R'). (d) Most slip occurs on through going PDS bands oriented sub-parallel to the zone axis.

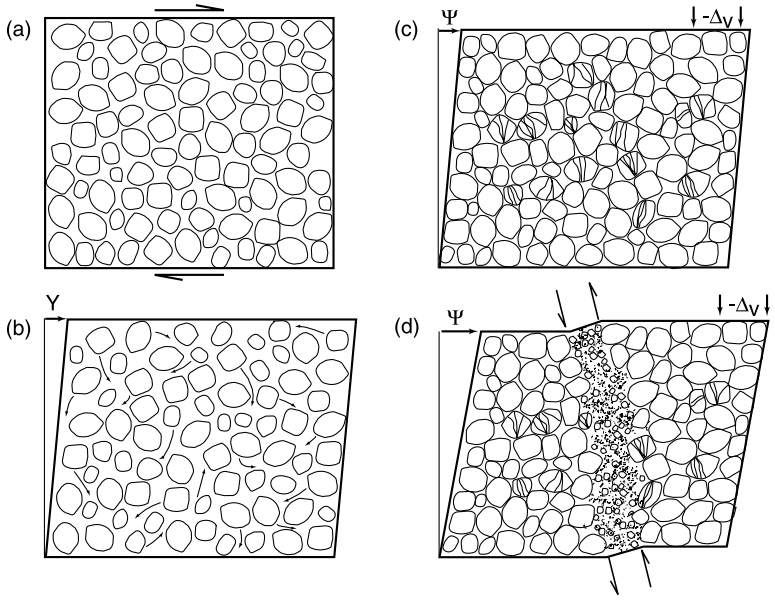

Fig. 11. Idealized sequential development of a Riedel shear zone in porous sandstone. (a) Undeformed, fluid-saturated sandstone is subjected to dextral shearing. (b) Elevated pore fluid pressure results in dilation and non-destructive particulate flow accompanied by angular shear ψ. (c) Continued shearing results in compaction and incipient cataclasis. The zone may also become work-hardened. (d) Cataclastic deformation on localized shear bands 1–2 grains wide. In Riedel shear zones, initial deformation occurs on high-angle, antithetic deformation bands (Z_1 bands). Modified after Lucas and Moore (1986, fig. 17).

that macroscale deformation within Sheets Gulch is not directly linked to structures in the underlying sedimentary and basement rocks. Likewise, the presence of smaller-scale, tip-to-tip PSZs suggests that these structures form in 'free' deformational space within the mechanically homogeneous Navajo Sandstone host. Thus the helicoidal geometry of antithetic deformation bands is more likely due to secondary localized reorientation of regional stresses along mesoscale PSZs (Davis et al., 2000), or to post-rupture rotation. As discussed, map-view exposures suggest there is strong evidence for distributed, two-dimensional shearing, and helicoidal deformation bands suggest that shearing was not restricted to a plane orthogonal to the strike of a PSZ or PRZ. Thus, it appears that these incipient bands propagate as planar features and are subsequently sheared in three dimensions, resulting in a three-dimensional helicoidal geometry.

6.2. A model for PRZ development

Field evidence suggests that the initiation and evolution of a PRZ includes both *non-destructive reorganization* of the Navajo Sandstone within the boundaries of the PRZ and localized *grain-scale cataclasis* within deformation bands. While it remains unproven at this time, perhaps shearing and compaction of this tabular deforming region induces locally elevated fluid pressure (Byerlee, 1990) which facilitates failure under low differential stress along the enigmatic, high-angle antithetic deformation bands, as well as passive deformation of these bands and sedimentary horizons by distributed, heterogeneous simple shear. This particular deformation path including elevated fluid pressure, distributed shearing, incipient cataclasis, and subsequent shear localization is consistent with interpretations of deformation within highly pressured porous sediments obtained from deep sea cores (Lucas and Moore, 1986) (Fig. 11). Increased fluid pressure within a deforming porous medium facilitates non-destructive reorganization and compaction, and in systems where differential stress is low, deformation may be distributed across a relatively broad region (Borradaile, 1981; Lucas and Moore, 1986). Eventually, distributed shearing becomes localized toward the center of the deforming zone (e.g. Mandl et al., 1977; Cundall, 1989), and the axis of the PRZ serves as a guide for further deformation manifested first as Riedel-array deformation bands, and, with sufficient strain, as a through-going fault zone (DBSZ).

6.3. Mechanisms of Z_1 and Z_2 band nucleation

Although a rigorous mechanical interpretation of Z_1 and Z_2 band nucleation is beyond the scope of this study, field evidence offers insight into possible formation mechanisms of these enigmatic features. As described, Z_1 and Z_2 elements are deformation bands, a type of shear fracture (Aydin, 1978), and in all observed examples they exhibit an antithetic sense of shear, as interpreted both from mesoscale field relationships and offset quartz grains in thin section. Both the antithetic shear sense of these bands and their steep inclination (55–85°) with respect to a PRZ axis is difficult to interpret mechanically, however. More importantly, it is unclear as to whether or not these initial deformation bands actually *nucleate* as shear fractures or if they nucleate as tensile fractures and *evolve* into shear

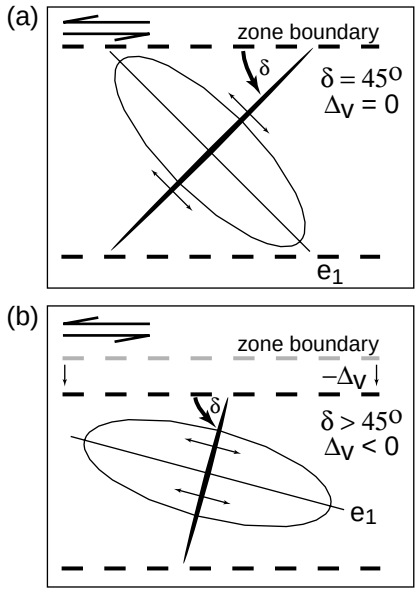

Fig. 12. The development of tensile fractures within a sinistral shear zone. (a) Constant volume deformation ($\Delta v = 0$); $\delta = 45°$, $e_1 = 45°$. (b) Net negative dilation of the shear zone ($\Delta v > 0$) (simple shear + pure shear); $\delta > 45°$, $e_1 < 45°$. Modified after Ramsay and Huber (1983, fig. 3.21).

fractures. In light of these questions, two other possible models for PRZ development must be considered.

The first model, in which Z_1 and Z_2 bands nucleate as tensile fractures and are subsequently reactivated as shear fractures, is motivated by the striking geometric similarity between PRZs and tension fracture arrays (e.g. Shainin, 1950, plates 1 and 2). Ideally, a tensile fracture array is a roughly tabular zone of en échelon tensile fractures that nucleate at $\delta \approx 45°$, where δ is the angle of an individual fracture with respect to the trend of the zone (e.g. Hancock, 1972). The angle δ is dependent on a number of factors including the relative volume change of the shearing zone during fracture propagation. For example, if the shear zone positively dilates during deformation, δ will be less than 45°, and if the zone compacts during deformation, δ will be greater than 45° (e.g. Ramsay and Huber, 1983, fig. 3.21) (Fig. 12) which is consistent with all observed PRZs (Z_1 and Z_2 bands show $55° \leq \delta \leq 90°$). There is ample field evidence suggesting that heterogeneous simple shear is an important component in PRZ development, as is suggested by other workers to explain sigmoidal gash fracture arrays (e.g. Roering, 1968). It is also possible that these arrays develop without simple shear under a locally modified stress field (Latjai, 1969; Nicholson and Pollard, 1985; Olson and Pollard, 1991), but the model does not apply to systems such as PRZs where $\delta > 50°$.

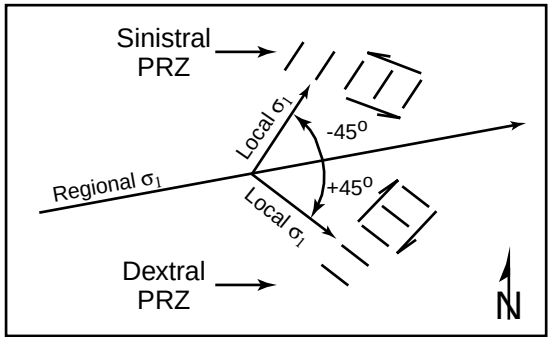

Fig. 13. Schematic representation of regional σ_1 rotation within PRZs if Z_1 bands nucleate as tensile fractures. The expected rotation is approximately +45° for dextral PRZs and −45° for sinistral PRZs (clockwise rotation is positive). The figure is representative of observed PRZs and regional stress interpreted by Davis et al. (2000) within the Sheets Gulch area.

Although the model is attractive geometrically, it is mechanically unintuitive, as it requires a significant local stress rotation to generate the initial elements, and subsequent stress 'unrotation' to drive slip along these elements. PRZs are oriented similarly to a sub-regional, conjugate set of DBSZs (Davis et al., 2000), and are interpreted to form similarly in a conjugate fashion. Davis et al. (2000) demonstrate a need for minor, localized anticlockwise stress rotation along sinistral DBSZs and localized clockwise stress rotation along dextral DBSZs, but the formation of Z_1 and Z_2 bands as tensile fractures requires a more drastic, ~45° local rotation of the principal stress along PRZs (Fig. 13). Thus, it seems unlikely that Z_1 and Z_2 bands nucleate as tension fractures and subsequently become reactivated as shear fractures.

Alternatively, these incipient deformation bands could form as hybrid shear-extensional (transitional tensile) fractures, which would be kinematically compatible with localized stress fields proposed by Davis et al. (2000). In this model, a tensile stress component along Z_1 and Z_2 bands reduces grain-to-grain contacts and facilitates shear failure, as suggested by other workers analyzing similar features (Rickard and Rixon, 1983; Davis, pers. commun., 1998). Despite the geometric and kinematic compatibility of Z_1 and Z_2 bands with this model, however, Engelder (1999) argues convincingly that hybrid shear-extensional fractures are not likely to be found in natural systems. This, the exact genesis of initial deformational elements comprising PRZs remains inconclusive.

7. Conclusions

This study documents a new style of Riedel shear zone evolution through interpretation of outcrop exposures in the Navajo Sandstone of southern Utah. Small-scale Riedel shear zones display consistent along-strike transitions from simple, incipient geometries to more complex Riedel-type geometries. Antithetic driven Riedel shear zones nucleate as Proto-Riedel Zones (PRZs) composed of spaced Z_1 and Z_2 deformation bands localized within a tabular, shearing zone of Navajo Sandstone. These initial shears are oriented at a high acute angle to the trend of the PRZ and have an antithetic sense of shear. Further strain is accommodated by distributed shear across the breadth of the

zone, which sigmoidally deforms the initial deformation bands. The zone is subsequently overprinted by a pair of conjugate deformation bands consistent with a Riedel-type geometry, and with further shearing, the region may evolve into a through-going fault zone.

Although the mechanics of this antithetic driven system are unclear, the initial high-angle features likely develop as Coulomb shear fractures. At sufficiently high levels of shear strain, strain localizes toward the axis of the PRZ and conjugate Z_3 and Z_4 deformation bands develop, transforming the PRZ into a Principal Shear Zone (PSZ). These bands are consistent with R and R' bands in Riedel-type shear zones, and nucleate symmetrically about a local σ_1.

The internal geometry of a Riedel shear zone is visualized and clarified by a detailed, three-dimensional digital reconstruction of a field sample. This modeling technique may be applied effectively to other structural systems with far-ranging applications, especially in hydrological and petroleum exploration/production. For example, petroleum reservoirs are often compartmentalized by smaller-scale structural elements such as deformation bands that are difficult to image but have a profound impact on subsurface fluid movement. High-resolution geometric modeling of analog exposures, such as those at Sheets Gulch, provides important insight into the shapes, extents, and connectivity of the structures comprising the compartments. Furthermore, the integration of geometric modeling with a temporal understanding of structural development provides insight into how a reservoir becomes progressively compartmentalized, which may assist with exploration and production efforts within the reservoir.

Acknowledgements

This study was supported financially in part by grants from (in alphabetical order) Amoco, Arco, Midland Valley Exploration, and Sigma Xi GIAR. I am indebted to Midland Valley Exploration for providing ***2D**Move*™ and ***3D**Move*™ software through the GeoStructure Partnership at the University of Arizona, David Woody for assisting in the field, and Dave Streeter for providing open access to the rock mechanics facilities in the Department of Mining and Geological Engineering at the University of Arizona. This manuscript benefited greatly from thorough reviews by Alex Bump, Lori Kennedy, and Jim Evans. I am also thankful for insightful conversations with George Davis and Peter Hennings.

References

Ahlgren, S.G., 1999. New interpretations of the sequential development of three dimensional deformation band shear zone networks in the Navajo Sandstone, southern Utah. The American Association of Petroleum Geologists 1999 Annual Convention Abstracts with Programs 8, A2.

Antonellini, M., Aydin, A., 1994. Effect of faulting on fluid flow in porous sandstones: petrophysical properties. The American Association of Petroleum Geologists Bulletin 78, 355–377.

Aydin, A., 1978. Small faults formed as deformation bands in sandstone. Pure and Applied Geophysics 116, 913–930.

Aydin, A., Johnson, A.M., 1983. Analysis of faulting in porous sandstones. Journal of Structural Geology 5, 19–31.

Bartlett, W.L., Friedman, M., Logan, J.M., 1981. Experimental folding and faulting of rocks under confining pressure. Part IX. Wrench faults in limestone layers. Tectonophysics 79, 255–277.

Billingsley, G.H., Huntoon, P.W., Breed, W.J., 1987. Geologic map of Capitol Reef National Park and vicinity, Utah. Utah Geological and Mineral Survey.

Borradaile, G.J., 1981. Particulate flow of rock and the formation of cleavage. Tectonophysics 72, 305–321.

Braun, J., 1994. Three-dimensional numerical simulations of crustal-scale wrenching using a non-linear failure criterion. Journal of Structural Geology 16, 1173–1186.

Bump, A., Ahlgren, S.G., Davis, G.H., 1997. The Waterpocket fold, a tale of two uplifts, Capitol Reef National Park, Utah. EOS, Transactions of the American Geophysical Union 78, F701.

Byerlee, J.D., 1990. Friction, overpressure and fault normal compression. Geophysical Research Letters 7, 2109–2112.

Byerlee, J.D., 1992. The change in orientation of subsidiary shears near faults containing pore fluid under high pressure. Tectonophysics 211, 295–303.

Cloos, E., 1955. Experimental analysis of fracture patterns. Geological Society of America Bulletin 66, 241–256.

Cundall, P.A., 1989. Numerical experiments on localization in frictional materials. Ingeniur-Archiv 59, 148–159.

Davis, G.H., 1996. "Riedel relays" in deformation band shear zones, Colorado Plateau, Utah. Geological Society of America Abstracts with Programs 28, A-188.

Davis, G.H., Bump, A.P., Garcia, P.E., Ahlgren, S.G., 2000. Conjugate Riedel deformation band shear zones. Journal of Structural Geology 22, 169–190.

Davis, G.H., Garcia, P., Bump, A.P., Ahlgren, S.G., Swanberg, K., 1997. Detailed internal structure of a conjugate strike–slip deformation band shear zone system in the Navajo Sandstone at a salient in the Waterpocket Fold, Capitol Reef National Park, Utah. EOS, Transactions of the American Geophysical Union 78, F701.

Dengo, C.A., Logan, J.M., 1979. Correlation of fracture patterns in natural and experimental shear zones. EOS, Transactions of the American Geophysical Union 60, 955.

Dresan, G., 1991. Stress distribution and the orientation of Riedel shears. Tectonophysics 188, 239–247.

Emmons, R.C., 1969. Strike–slip rupture patterns in sand models. Tectonophysics 7, 71–87.

Engelder, T., 1999. Transitional-tensile fracture propagation: a status report. Journal of Structural Geology 21, 1049–1055.

Gamond, J.F., 1983. Displacement features associated with fault zones: a comparison between observed examples and experimental models. Journal of Structural Geology 5, 33–45.

Garcia, P., Davis, G.H., 1997. Detailed internal structure of a conjugate normal deformation band shear zone system in the Navajo Sandstone at the northern end of the East Kaibab Monocline, southern Utah. EOS, Transactions of the American Geophysical Union 78, F702.

Gibbs, A.D., 1990. Towards a three dimensional approach to restoration and modelling of geological structure. In: Oil and Gas Technology in a Wider Europe, 4th EC Symposium. Commission of the European Communities Directorate-General for Energy, Brussels, pp. 211–220.

Gibbs, A.D., Griffiths, P.A., 1996. 3D Kinematic structural restoration and its impact on reduction of risk—new techniques arising from commercialisation of software developed for three dimensional volume balanced analysis of geological structure. In: Strategic Importance of Oil and Gas Technology, 5th EU Hydrocarbons Symposium. Commission of the European Communities Directorate-General for Energy, Brussels, pp. 272–282.

Hancock, P.L., 1972. The analysis of *en-echelon* veins. Geological Magazine 109, 269–276.

Hildebrand-Mittlefehldt, N., 1979. Deformation near a fault termination, part I: a fault in a clay experiment. Tectonophysics 57, 131–150.

Hills, E.S., 1963. Elements of Structural Geology. Methuen, London.

Hintze, L.F., 1988. Geologic History of Utah. Department of Geology, Brigham Young University.

Kelley, V.C., 1955. Tectonics of the Colorado Plateau in Relationship to the Origin and Distribution of Uranium. The University of New Mexico, Albequerque.

Kiersch, G.A., 1950. Small-scale structures and other features of Navajo Sandstone, northern part of the San Rafael Swell, Utah. The American Association of Petroleum Geologists Bulletin 34, 923–942.

Latjai, E.Z., 1969. Mechanics of second-order faults and tension gashes. Geological Society of America Bulletin 80, 2253–2272.

Lucas, S.E., Moore, J.C., 1986. Cataclastic deformation in accretionary wedges: Deep Sea Drilling Project Leg 66, southern Mexico, and on-land examples from Barbados and Kodiak Islands. In: Moore, J.C. (Ed.). Structural Fabrics in Deep Sea Drilling Project Cores from Forearcs. Geological Society of America Memoir 166The Geological Society of America, pp. 89–103.

Maltman, A., 1987. Shear zones in argillaceous sediments—an experimental study. In: Jones, M.E., Preston, R.M.F. (Eds.). Deformation of Sediments and Sedimentary Rocks. Geological Society Special Publication 29, pp. 77–87.

Mandl, G., 1988. Mechanics of Tectonic Faulting. Models and Basic Concepts. Elsevier, Amsterdam.

Mandl, G., de Jong, L.N.J., Maltha, A., 1977. Shear zones in granular material. Rock Mechanics 9, 95–144.

Marone, C., Scholz, C.H., 1989. Particle-size distribution and microstructures within simulated fault gouge. Journal of Structural Geology 11, 799–814.

McKinnon, S.D., Garrido de la Barra, I., 1998. Fracture initiation, growth and effect on stress field: a numerical investigation. Journal of Structural Geology 20, 1673–1689.

Moore, D., Byerleee, J., 1991. Comparison of the San Andreas fault, California, and laboratory fault zones. Geological Society of America Bulletin 103, 762–774.

Moore, D.E., Byerlee, J., 1992. Relationships between sliding behavior and internal geometry of laboratory fault zones and some creeping and locked strike–slip faults of California. Tectonophysics 211, 305–316.

Moore, J.M., 1979. Tectonics of the Najd transcurrent fault system, Saudi Arabia. Journal of the Geological Society of London 136, 441–454.

Morgenstern, N.R., Tchalenko, J.S., 1967. Microscopic structures in kaolin subjected to direct shear. Geotechnique 17, 309–328.

Morrow, C.A., Byerlee, J.D., 1989. Experimental studies of compaction and dilatancy during frictional sliding on faults containing gouge. Journal of Structural Geology 11, 815–825.

Naylor, M.A., Mandl, G., Sijpesteijn, C.H.K., 1986. Fault geometries in basement-induced wrench faulting under different initial stress states. Journal of Structural Geology 8, 737–752.

Nicholson, R., Pollard, D.D., 1985. Dilation and linkage of echelon cracks. Journal of Structural Geology 7, 583–590.

Olson, J.E., Pollard, D.D., 1991. The initiation and growth of en echelon veins. Journal of Structural Geology 13, 595–608.

Peacock, D.C.P., 1991. Displacements and segment linkage in strike–slip fault zones. Journal of Structural Geology 13, 1025–1035.

Pollard, D.D., Segall, P., Delaney, P.T., 1982. Formation and interpretation of dilatant echelon cracks. Geological Society of America Bulletin 93, 1291–1303.

Ramsay, J.G., Huber, M.I., 1983. The Techniques of Modern Structural Geology. Volume 1: Strain Analysis. Academic Press, London.

Ramsay, J.G., Huber, M.I., 1987. The Techniques of Modern Structural Geology. Volume 2: Folds and Fractures. Academic Press, London.

Rickard, M.J., Rixon, L.K., 1983. Stress configuration in conjugate quartz-vein arrays. Journal of Structural Geology 5, 573–578.

Riedel, W., 1929. Zur mechanik geologischer brucherscheinungen. Zentralblatt für Mineralogie, Geologie und paleontologie B, 354–368.

Roering, C., 1968. The geometrical significance of natural en-echelon crack arrays. Tectonophysics 5, 107–123.

Schreurs, G., 1994. Experiments on strike–slip faulting and block rotation. Geology 22, 567–570.

Segall, P., Pollard, D.D., 1980. Mechanics of discontinuous faults. Journal of Geophysical Research 85, 4337–4350.

Shainin, V.E., 1950. Conjugate sets of en echelon tension fractures in the Athens Limestone at Riverton, Virginia. Geological Society of America Bulletin 61, 509–517.

Skempton, A.W., 1966. Proceeedings of the International Congress on Rock Mechanics, 1st Lisbon, vol. 1, pp. 329–335.

Tanner, W.F., 1962. Surface structural patterns obtained from strike–slip models. Journal of Geology 70, 101–107.

Tchalenko, J.S., 1968. The evolution of kink-bands and the development of compression textures in sheared clays. Tectonophysics 6, 159–174.

Tchalenko, J.S., 1970. Similarities between shear zones of different magnitudes. Geological Society of America Bulletin 81, 1625–1640.

Tchalenko, J.S., Ambraseys, N.N., 1970. Structural analysis of the Dasht-e Bayaz (Iran) earthquake fractures. Geological Society of America Bulletin 81, 41–60.

Wilcox, R.E., Harding, T.P., Seely, D.R., 1973. Basic wrench tectonics. The American Association of Petroleum Geologists Bulletin 57, 74–96.